J. Plasma Physics (2014), *vol.* 80, *part* 1, *pp.* 27–41. © Cambridge University Press 2013
doi:10.1017/S0022377813000883

Two-dimensional nonlinear cylindrical equilibria with reversed magnetic shear and sheared flow

AP Kuiroukidis[1] and G. N. Throumoulopoulos[2,]†

[1]Technological Education Institute of Serres, 62124 Serres, Greece
[2]Department of Physics, University of Ioannina, Association Euratom-Hellenic Republic, GR 451 10 Ioannina, Greece

(Received 20 May 2013; revised 7 July 2013; accepted 9 July 2013; first published online 12 November 2013)

Nonlinear translational symmetric equilibria with up to quartic flux terms in free functions, reversed magnetic shear, and sheared flow are constructed in two ways: (i) quasi-analytically by an ansatz, which reduces the pertinent generalized Grad–Shafranov equation to a set of ordinary differential equations and algebraic constraints which is then solved numerically, and (ii) completely numerically by prescribing analytically a boundary having an X-point. This latter case presented in Sec. 4 is relevant to the International Thermonuclear Experimental Reactor project. The equilibrium characteristics are then examined by means of pressure, safety factor, current density, and electric field. For flows parallel to the magnetic field, the stability of the equilibria constructed is also examined by applying a sufficient condition. It turns out that the equilibrium nonlinearity has a stabilizing impact, which is slightly enhanced by the sheared flow. In addition, the results indicate that the stability is affected by the up-down asymmetry.

1. Introduction

Sheared flows play a role in the transitions to improve confinement regimes in magnetic confinement devices, as the L-H transition and the formation of internal transport barriers (ITBs), although understanding the physics of these transitions remains incomplete. In particular, magnetohydrodynamic (MHD) equilibria with flow, which is the basis of stability and transport studies, have been constructed as solutions to the generalized Grad–Shafranov equations, e.g. (1) as given below, (Mashke and Perrin 1984-Kuiroukidis and Throumoulopoulos 2013). In connection with the present study, we refer to our recent contribution (Kuiroukidis and Throumoulopoulos 2013), in which up-down symmetric nonlinear two-dimensional cylindrical equilibria with incompressible flow pertinent to the L-H transition were obtained. Equilibria relevant to the L-H transition usually have peaked toroidal current density profiles and safety factors increasing monotonically from the magnetic axis to the plasma boundary.

A necessary requirement for tokamak operation in connection with the International Thermonuclear Experimental Reactor (ITER) and DEMOnstration Power Plant (DEMO) projects is a constant toroidal plasma current which produces the poloidal component of the magnetic field. Among the different options for such non-inductive current drive (e.g. electron-cyclotron current drive, neutral beam current drive, bootstrap current) only the bootstrap current can produce a sufficiently large amount of toroidal current in big tokamaks. The amount of bootstrap current is proportional

† Email address for correspondence: gthroum@uoi.gr

https://doi.org/10.1017/S0022377813000883 Published online by Cambridge University Press

to the pressure gradient. Typically, the maximal pressure gradients are located off-axis, thus leading to hollow current profiles in the plasma associated with reversed magnetic shear. Static equilibria with reversed magnetic shear were the subject of Bellan (2002) and Martins et al. (2011).

The stability of fluids and plasmas in the presence of equilibrium flows non-parallel to the magnetic field remains a tough problem reflecting to the lack of necessary and sufficient conditions. Only for parallel flows few sufficient conditions for linear stability are available (Friedlander and Vishik 1995-Throumoulopoulos and Tasso 2007). We have found in previous studies that the stability condition of Throumoulopoulos and Tasso (2007) is not satisfied for the linear equilibria of Apostolaki et al. (2008) and Throumoulopoulos and Tasso (2012), while it is satisfied within an appreciable part of the plasma for the nonlinear equilibria of Throumoulopoulos et al. (2009), Throumoulopoulos and Tasso (2010), and Kuiroukidis and Throumoulopoulos (2013). This led us to the conjecture that the equilibrium nonlinearity may act synergetically with the sheared flow to stabilize the plasma.

Aim of the present study is to extend our previous paper (Kuiroukidis and Throumoulopoulos 2013) in two respects: up-down asymmetry, and reversed magnetic shear. As in Kuiroukidis and Throumoulopoulos (2013), non-magnetic field-aligned equilibrium flows will be included. In this respect a synergism of reversed magnetic shear and sheared poloidal and toroidal rotation, consisting of on the one hand the reversed magnetic shear, which plays a role in triggering the ITBs' development, and the sheared rotation, on the other hand, which has an impact on the subsequent growth and allows the formation of strong ITBs, was observed in JET (de Vries et al. 2009) and DIII-D (Shafer et al. 2009). In addition, here the above conjecture about the combination of stabilizing effects of equilibrium nonlinearity and plasma flow will be checked. The reason for considering translational symmetry is the many free physical and geometrical parameters involved in connection with flow amplitude, direction and shear, equilibrium nonlinearity, symmetry, and toroidicity. Thus, in the presence of nonlinearity one could first exclude toroidicity. The reader is also referred to the introduction of our previous paper (Kuiroukidis and Throumoulopoulos 2013).

The organization of the paper is as follows: In the second section we present the equilibrium equations governing translationally symmetric equilibria with incompressible flow and introduce the ansatz reducing the problem to a set of ordinary differential equations (ODEs) and algebraic constraints. In Sec. 3, up-down asymmetric equilibria are constructed quasi-analytically and their characteristics are studied. In Sect. 4, equilibria with a lower X-point are derived numerically by imposing analytically the boundary shape. A stability consideration of the equilibria obtained is made in Sec. 5, and Section 6 summarizes the conclusions.

2. Translational symmetric equilibria with flow

The equilibrium of a cylindrical plasma with incompressible flow and arbitrary cross-sectional shape satisfies the generalized Grad–Shafranov equation (Throumoulopoulos and Tasso 1997; Simintzis et al. 2001),

$$\left(1-M_p^2\right)\nabla^2\psi-\frac{1}{2}\left(M_p^2\right)'|\nabla\psi|^2+\frac{d}{d\psi}\left(\mu_0 P_s+\frac{B_z^2}{2}\right)=0 \tag{1}$$

for the poloidal magnetic flux function ψ and the Bernoulli relation for the pressure

$$P=P_s(\psi)-\frac{1}{2\mu_0}M_p^2(\psi)|\nabla\psi|^2. \tag{2}$$

https://doi.org/10.1017/S0022377813000883 Published online by Cambridge University Press

Here $M_p(\psi)$, $P_s(\psi)$, $\rho(\psi)$, and $B_z(\psi)$ are respectively the poloidal Alfvén Mach function, pressure in the absence of flow, matter density and magnetic field parallel to the symmetry axis z, which are surface quantities. Because of the symmetry, the equilibrium quantities are z-independent and the axial velocity v_z does not appear explicitly in (1). SI units are employed unless otherwise stated (see Sec. 5). Derivation of (1) and (2) is briefly outlined in Sec. 2 of Kuiroukidis and Throumoulopoulos (2013). Details are provided in Throumoulopoulos and Tasso (1997) and Simintzis et al. (2012). Because of the flow, P is not a surface quantity. Also the density becomes surface quantity because of incompressibility. Five of the surface quantities chosen here as P_s, ρ, B_z, M_p^2, and v_z remain arbitrary (can be freely chosen).

Using the mapping

$$u(\psi) = \int_0^{\psi} [1 - M_p^2(g)]^{1/2} dg, \quad (M_p^2 < 1), \tag{3}$$

(1) is transformed to

$$\nabla^2 u + \frac{d}{du}\left(\mu_0 P_s + \frac{B_z^2}{2}\right) = 0. \tag{4}$$

Note that transformation (3) does not affect the magnetic surfaces, it just relabels them. Equation (4) is identical in form with the static equilibrium equation.

In the present study we assign the free function term in (4) as

$$\left(\mu_0 P_s + \frac{B_z^2}{2}\right) = c_0 + c_1 u + c_2 \frac{u^2}{2} + c_3 \frac{u^3}{3} + c_4 \frac{u^4}{4} \tag{5}$$

to obtain

$$u_{xx} + u_{yy} + c_1 + c_2 u + c_3 u^2 + c_4 u^3 = 0, \tag{6}$$

where (x, y) are the usual Cartesian coordinates. The form of this equation leads us to introduce the following up-down asymmetric ansatz for the flux function which enables reduction of the equilibrium problem to a set of ODEs and first-order constraints:

$$u = \frac{N_2(x) y^2 + N_1(x) y + f(x) D_0(x)}{y^2 + D_1(x) y + D_0(x)}. \tag{7}$$

This is an extension of the respective ansatz for up-down symmetric equilibria that we introduced for the first time in Kuiroukidis and Throumoulopoulos (2013). Inserting (7) into (6), after a rather lengthy calculation, the latter is transformed into a fraction (F), the nominator of which is a polynomial of y of sixth order. Equating this nominator to zero, from the y^6-term we obtain

$$N_2'' + c_1 + c_2 N_2 + c_3 N_2^2 + c_4 N_2^3 = 0. \tag{8}$$

From the y^0-term it follows

$$f'' + \frac{2(N_2 - f)}{D_0} - \frac{2D_1(N_1 - f D_1)}{D_0^2} + c_1 + c_2 f + c_3 f^2 + c_4 f^3 = 0. \tag{9}$$

From the y, y^4, y^5-terms, one yields

$$N_1'' = \frac{1}{DD}\big[- N_2(N_2 - f)G_1 + (f D_0^2 (N_2 - f) - D_0(N_1 - f D_1)(N_1 + N_2 D_1))G_5 + D_0 N_2 (N_1 - f D_1) G_4\big], \tag{10}$$

https://doi.org/10.1017/S0022377813000883 Published online by Cambridge University Press

$$D_1^{''} = \frac{1}{DD}\left[-(N_2 - f)G_1 + (D_0^2(N_2 - f) - 2D_0D_1(N_1 - fD_1))G_5 + D_0(N_1 - fD_1)G_4\right], \tag{11}$$

$$D_0^{''} = \frac{1}{DD}\left[(N_1 - N_2D_1)G_1 - D_0^2(N_1 + N_2D_1 - 2fD_1)G_5 + D_0^2(N_2 - f)G_4\right], \tag{12}$$

where $DD = D_0(N_1 - fD_1)(N_1 - N_2D_1) + D_0^2(N_2 - f)^2$ and the functions G_1, G_4, and G_5 are given in the Appendix. From the y^3, y^2 terms we obtain respectively the first-order constraints C_1, C_2,

$$\begin{aligned}&(D_1^2 + 2D_0)N_1^{''}(\phi, \phi^{'}) - (N_1 + N_2D_1 - 2fD_1)D_0^{''}(\phi, \phi^{'})\\ &\quad -(N_2D_0 + N_1D_1 + fD_0)D_1^{''}(\phi, \phi^{'}) + G_3 = 0\end{aligned} \tag{13}$$

and

$$\begin{aligned}&2D_0D_1N_1^{''}(\phi, \phi^{'}) - (D_0(N_2 - f) + D_1(N_1 - fD_1))D_0^{''}(\phi, \phi^{'})\\ &\quad - D_0(N_1 + fD_1)D_1^{''}(\phi, \phi^{'}) + G_2 = 0.\end{aligned} \tag{14}$$

Here ϕ denotes collectively all the functions appearing in (7), and (10)–(12) are used. The functions G_2, G_3 are also given in the Appendix. Note that (13) and (14) are not the second-order 'evolution' differential equations but rather the first-order constraints to be fulfilled during numerical integration. This justifies the introduction of ansatz (7), which results in a simple numerical treatment of the equilibrium through ODEs and algebraic constraints in contrast and alternative to the full numerical treatment of Sec. 4.

3. Class of quasi-analytic solutions

The system of (8)–(12) is integrated numerically using high-precision numerical integration with very small step size due to its extreme complexity and nonlinearity. The magnetic axis regularized with respect to the geometric centre is taken to be 'Shafranov shifted'‡ at $x_a = 1 + x_s = 1.1$. We take the following ITER-pertinent geometrical data: $a = 2$ m, $R_0 = 6.2$ m for the minor and major radius of the 'torus' respectively, and the inverse aspect ratio is $\epsilon_0 = 0.32$. The bounds for the x-variable are $x_{\min} = 1 - \epsilon_0$ and $x_{\max} = 1 + \epsilon_0$. The integration begins from x_a forward up to $x_{\max}$ and backwards up to $x_{\min}$. For the following values of the parameters $c_1 = 52.0$, $c_2 = -0.4$, $c_3 = 0.1$, and $c_4 = 0.1$ and for initial conditions $N_2 = -1.4$, $N_2^{'} = 0.95$, $N_1 = -0.15$, $N_1^{'} = -1.05$, $D_1 = 0.15$, $D_1^{'} = -0.137$, $D_0 = 1.05$, $D_0^{'} = 0.1$, $f = 7.5$, and $f^{'} = 0.0$ we obtained the solution of Fig. 1. The first-order constraints of (13)–(14) were monitored during the integration and they were kept to very low values. The product of the constraint C_1 with the average value of y^3 (taken to be equal to 0.2) and the constraint C_2 with the average value of y^2 that appear in the nominator of the final fraction (F) (see the text just below (7)) were kept bounded to $|C_1| \leqslant 0.07$ and $|C_2| \leqslant 0.18$. This combined with the fact that the denominator of this fraction has a positive definite value greater or equal to 1.0 is an additional argument that this fraction is very close to zero and that the presented equilibrium is indeed an acceptable solution of (6).

‡ Here the term 'Shafranov shift' means that the equilibrium, in addition to up-down is left-right asymmetric and is not connected to the toroidicity that vanishes in cylindrical geometry.

https://doi.org/10.1017/S0022377813000883 Published online by Cambridge University Press

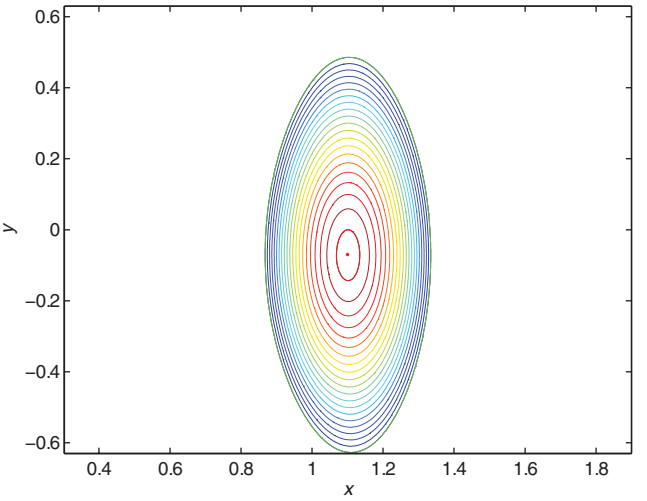


FIGURE 1. (Colour online) Equilibrium for the initial conditions given in the text of Sec. 2. The bounding surface, corresponds to $u_b = 5.5$ Wb, while at the magnetic axis, which is located at $(x_a, y_a) = (1.1, -0.07)$, $u_a = 7.8$ Wb.

The bounding surface (shown in green) corresponds to $u_b = 5.5$ Wb, while the magnetic axis corresponds to $u_a = 7.8$ Wb. The magnetic axis is located at $(x_a, y_a) = (1.1, -0.07)$. A quartic fitting yields expressions for the functions N_2, N_1, D_1, D_0, f such as the following equation

$$N_2 = 5.527x^4 - 23.78x^3 + 11.81x^2 + 31.95x - 27.27. \tag{15}$$

We, however, stress the fact that for a correct representation and plotting of various functions, all the higher order expansions and more precise numerical parametric values are needed. Plotting (7) using (15) will *not* yield the correct result of Fig. 1, which occurs through the precise numerical results for these functions.

The MHD safety factor is defined as (Wesson 2011)

$$q(u) = \frac{d\psi_{\rm tor}/dV}{d\psi_{\rm pol}/dV} = \frac{1}{2\pi}\frac{d\psi_{\rm tor}/dV}{d\psi/dV}. \tag{16}$$

Using $dV = 2\pi|J|d\psi d\theta$, $J^{-1} = \nabla\theta \cdot (\nabla\phi \times \nabla\psi)$ and expressing the fluxes in terms of the magnetic field, one can cast (16) in the form of a line integral on each constant$-u$ curve. The detailed evaluation of q for the present equilibrium of Fig. 1 yields the curve of Fig. 2 with strong reversed magnetic shear. For this result it was used $c_0 = 200.0$ in (5). Also, for the axial magnetic field it adopted the typical tokamak diamagnetic function $B_z = B_{z0}(1 + \gamma(1 - \frac{u}{u_b}))$, as shown in Fig. 3, with $\gamma = 0.1$ and $B_{z0} = 3.2$ T . Then the static pressure function $P_s(u)$ is computed by (5), while for the flow function in (3) it was used $M_p^2 = M_{pa}(\frac{u}{u_b} - 1)^{2.5}$ with $M_{pa} = 0.1$ and $u_b = 5.5$ Wb $\leqslant u \leqslant u_a = 7.5$ Wb. The pressure (2) is shown in Fig. 4, normalized to its centre value of $P_0 = 2.1046 \times 10^5$ Pa. Also, instead of the axial velocity v_z, the corresponding Mach function M_z^2 is chosen similar to the poloidal one ($M_z^2 \simeq M_p^2$) with $M_{za} = 1.1\ M_{pa}$.

The electric field for equilibrium of Fig. 1 is shown in Fig. 5. Here the choice $\rho = \rho_a(\frac{u}{u_b} - 1)^{0.5}$ has been made for the density with $\rho_a = 4.0 \times 10^{-7}$ Kgr m^{-3}. The maximum of $\mathbf{E}$ increases with the flow parameter M_{pa} but the position of the maximum is not affected by the flow in agreement with the results of Simintzis et al.

https://doi.org/10.1017/S0022377813000883 Published online by Cambridge University Press

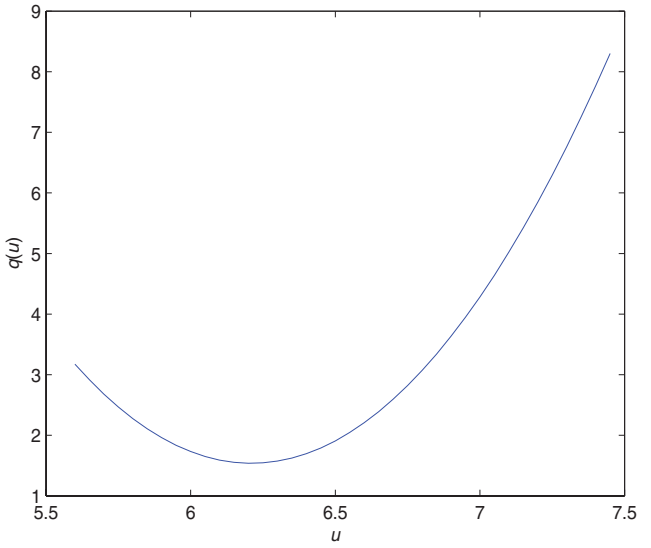


FIGURE 2. (Colour online) The safety factor for the equilibrium of Fig. 1 presenting a strong negative magnetic shear region. The outer bounding surface corresponds to $u = u_b = 5.5$ Wb, while at the magnetic axis $u = u_a = 7.5$ Wb.

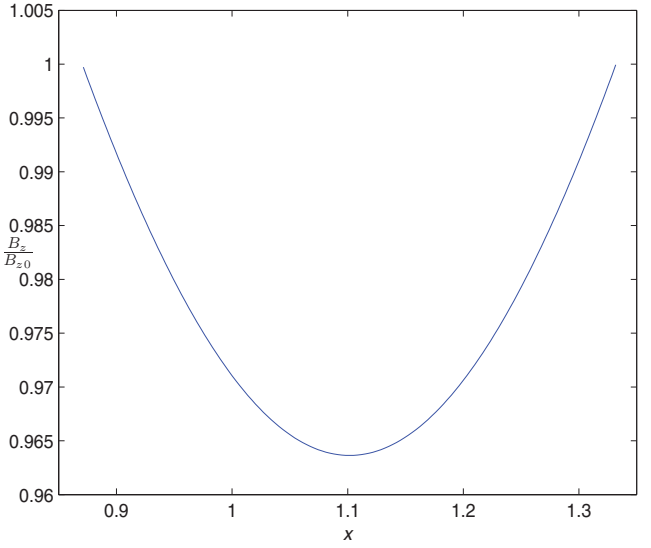


FIGURE 3. (Colour online) The axial magnetic field B_z, for equilibrium of Fig. 1 normalized to its centre value of $B_{z0} = 3.2$ T.

(2001) and Kuiroukidis and Throumoulopoulos (2012). The hollow axial current density profile in the midplane $y = 0$ is shown in Fig. 6 in consistence with the negative magnetic shear curve for the safety factor of Fig. 2.

4. Numerical asymmetric equilibrium with X-point

We now consider the direct numerical solution of (6) with a prescribed boundary possessing a divertor null X-point. We will first specify the boundary. The boundary

https://doi.org/10.1017/S0022377813000883 Published online by Cambridge University Press

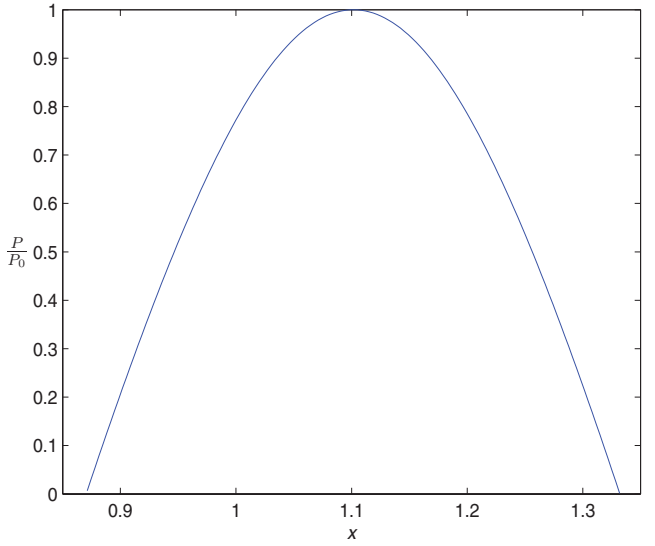


FIGURE 4. (Colour online) The pressure for equilibrium of Fig. 1 normalized to its centre value of $P_0 = 2.1046 \times 10^5$ Pa.

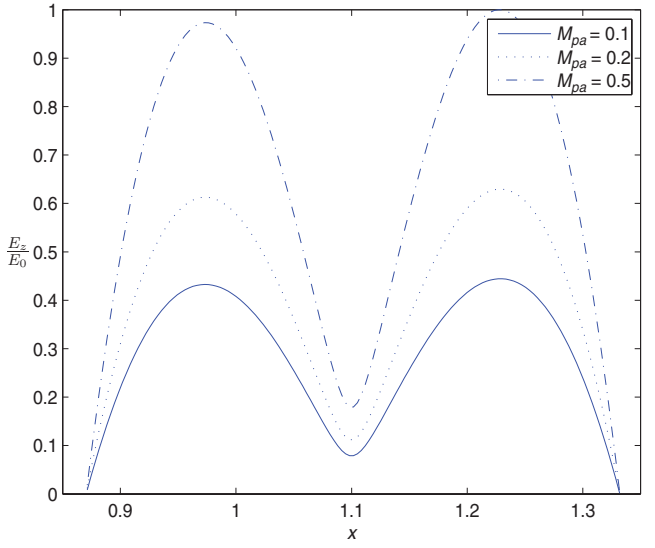


FIGURE 5. (Colour online) The electric field E_z, for equilibrium of Fig. 1 normalized to its maximum value of $E_0 = 5.4851\,\mathrm{kV\ m^{-1}}$.

conditions for the flux function u is $u_b = 1$ Wb on the prescribed boundary curve and $u_a = 0$ Wb on the magnetic axis. The magnetic axis is taken to be Shafranov shifted at $x_a = 1 + x_s = 1.1$. The model thus has three free parameters, which are the Shafranov shift x_s, the elongation κ, and the triangularity δ. Their values are taken as $x_s = 0.1$, $\kappa = 1.86$, and $\delta = 0.5$, in accordance with the corresponding data of the ITER project. The bounding flux surface for the asymmetric case is shown in Fig. 7. We take the values $a = 2\,\mathrm{m}$ and $R_0 = 6.2\,\mathrm{m}$ for the minor and major radius of the 'torus' respectively, for which the inverse aspect ratio is $\epsilon_0 = 0.32$.

https://doi.org/10.1017/S0022377813000883 Published online by Cambridge University Press

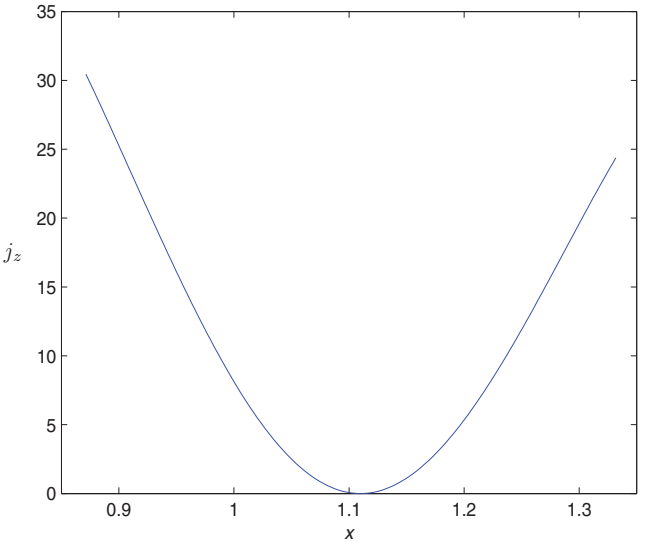


FIGURE 6. (Colour online) The axial current density at the midplane $A(x, y = 0)$ for the equilibrium of Fig. 1. It is hollow in connection with the negative magnetic shear of Fig. 2.

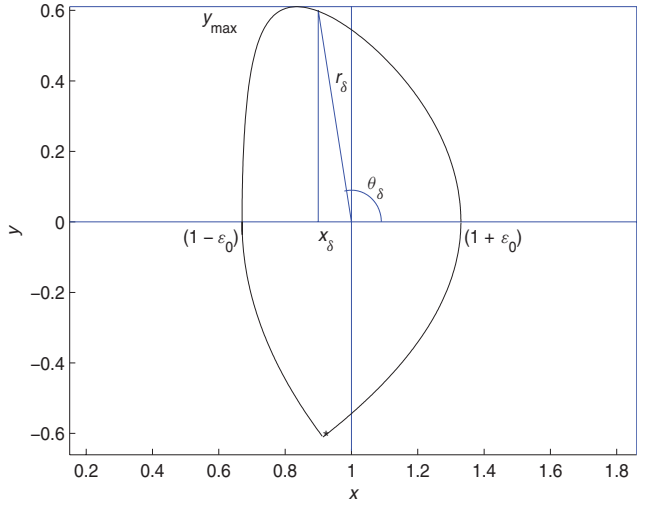


FIGURE 7. (Colour online) Bounding flux surface for the asymmetric case defined by (17)–(20), possessing a divertor, null X-point at $P_X(x_X, y_X) = (0.9139, -0.6105)$.

The equation for the upper part of the bounding flux surface, which if taken to hold for the lower part as well would give a symmetric bounding surface, is

$$x_b = 1 + \epsilon_0 \cos(\tau + \alpha \sin(\tau)), \quad y_b = y_{\max} \sin(\tau), \tag{17}$$

where $y_{\max} = \kappa\epsilon_0$ with $\delta = (1 - x_\delta)/\epsilon_0$, and $\alpha = \sin^{-1}(\delta)$. Thus, the following relations hold: $x_\delta = 1 - \delta\epsilon_0$ and $\theta_\delta = \pi - \tan^{-1}(\kappa/\delta)$. The parameter τ is any increasing function of the polar angle θ, satisfying $\tau(0) = 0$, $\tau(\pi) = \pi$, and $\tau(\theta_\delta) = \pi/2$. In our model we

https://doi.org/10.1017/S0022377813000883 Published online by Cambridge University Press

take

$$\tau(\theta) = t_0\theta^2 + t_1\theta^n, \quad t_0 = \frac{\theta_\delta^n - \frac{1}{2}\pi^n}{\pi\theta_\delta^n - \theta_\delta^2\pi^{n-1}}, \quad t_1 = \frac{-\theta_\delta^2 + \frac{1}{2}\pi^2}{\pi\theta_\delta^n - \theta_\delta^2\pi^{n-1}} \tag{18}$$

with $n = 8$. In order to complete the asymmetric bounding curve, we now specify the lower part of it ($y < 0$) as follows. The left lower branch of the curve is given by

$$\begin{aligned} x_b &= 1 + \epsilon_0\cos(\theta), \\ y_b &= -[2p_1\epsilon_0(1+\cos\theta)]^{1/2}, \\ p_1 &= \frac{y_{\max}^2}{2\epsilon_0(1+\cos\theta_\delta)}, \quad (\pi \leqslant \theta \leqslant 2\pi - \theta_\delta), \end{aligned} \tag{19}$$

while the right lower branch of the curve is given by

$$\begin{aligned} x_b &= 1 + \epsilon_0\cos(\theta), \\ y_b &= -[2p_2\epsilon_0(1-\cos\theta)]^{1/2}, \\ p_2 &= \frac{y_{\max}^2}{2\epsilon_0(1-\cos\theta_\delta)}, \quad (2\pi - \theta_\delta \leqslant \theta \leqslant 2\pi). \end{aligned} \tag{20}$$

The divertor null X-point is located at $x_X = 1 + \epsilon_0\cos\theta_\delta = 0.9139$ and $y_X = -y_{\max} = -0.6105$.

The Laplacian operator $u_{xx} + u_{yy}$ is discretized on a rectangular grid where we have $(1-\epsilon_0) \leqslant x \leqslant (1+\epsilon_0)$ and $-y_{\max} \leqslant y \leqslant y_{\max}$ with grid step h. The nine-point formula is then employed (Gerald and Wheatley 1989),

$$\begin{aligned} \nabla^2 u_{i,j} = \frac{1}{6h^2}\big[&u_{i+1,j+1} + 4u_{i+1,j} + u_{i+1,j-1} + 4u_{i,j+1} \\ &+ 4u_{i,j-1} + u_{i-1,j+1} + 4u_{i-1,j} + u_{i-1,j-1} - 20u_{i,j}\big] \end{aligned} \tag{21}$$

and when substituted into (6), the latter is written as $u_{i,j}^{(\mathrm{new})} = G(u)_{i,j}^{(\mathrm{old})}$ and is solved iteratively. The last term of (21) is taken to be the $u_{i,j}^{(\mathrm{new})}$ and the iterations stop (i.e. reaching convergence to the solution) when $|u_{i,j}^{(\mathrm{new})} - u_{i,j}^{(\mathrm{old})}| < 0.001$. We again stress that the conditions $u_b = 1$ on the boundary and $u_a = 0$ on axis are imposed in every iteration. For $h = 0.02$, and for the following values of the constants of (6), $c_1 = -10.0$, $c_2 = 2.0$, $c_3 = 1.1, c_4 = 1.1$, a number of $N = 165$ iterations were needed to obtain the desired accuracy. The solution is shown in Fig. 8. Although it seems that the solution is dependent on the specific value of the h chosen, from the discrete two-dimensional matrix of $u_{i,j}$ produced, a two-dimensional Lagrange fitting is performed that yields a polynomial in (x, y). This is h-independent. It is noted that the ripples of the flux function appearing near the boundary of the equilibrium are due to numerical instabilities that are inevitably present in the calculation.

5. A stability consideration

We now address the important issue of the stability of the solutions constructed with respect to small linear MHD perturbations by means of the sufficient condition of Throumoulopoulos and Tasso (2007). This condition concerning internal modes states that a general steady state of a plasma of constant density and incompressible flow parallel to **B** is linearly stable to small three-dimensional perturbations if the flow is sub-Alfvénic ($M_p^2 < 1$) and $A \geqslant 0$, where A is given below by (22). Consequently, using henceforth dimensionless quantities we set $\rho = 1$. Also, for parallel flows

https://doi.org/10.1017/S0022377813000883 Published online by Cambridge University Press

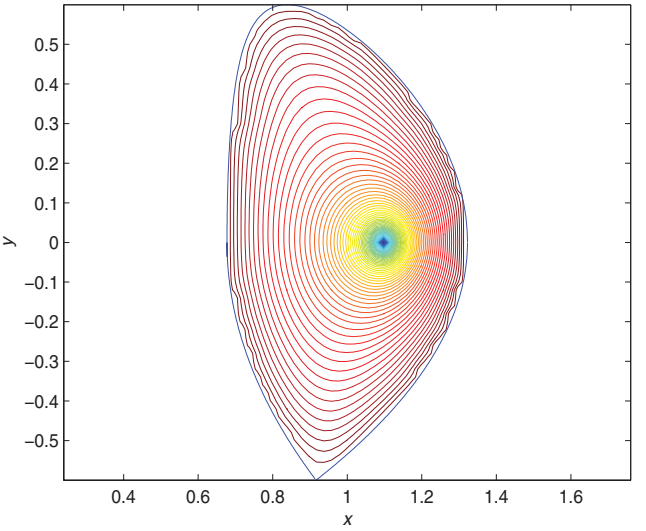


FIGURE 8. (Colour online) The numerical solution of (6) for the parameter values given in the text of Sec. 4.

($\mathbf{v} = M\mathbf{B}$) it holds $M_p \equiv M_z \equiv M$. In fact if the density is uniform at equilibrium it remains so at the perturbed state because of incompressibility. In the u-space for axisymmetric equilibria, A assumes the form

$$A = -\bar{g}^2\left[(\mathbf{j}\times\nabla u)\cdot(\mathbf{B}\cdot\nabla)\nabla u + \left(\frac{M_p^2}{2}\right)'\frac{|\nabla u|^2}{(1-M_p^2)^{3/2}}\left\{\nabla u\cdot\nabla(B^2/2) + \bar{g}\frac{|\nabla u|^2}{(1-M_p^2)^{1/2}}\right\}\right] \tag{22}$$

with

$$\bar{g} := \frac{P_s'(u) - (M_p^2)'B^2/2}{1-M_p^2}.$$

This condition, although complicated, is accurate (a proof is provided in Throumoulopoulos and Tasso 2007) and all the computations and conclusions have been performed with great care. Specifically, its application to the equilibria constructed in Secs. 3 and 4 led to the following results:

1. Even a weak up-down asymmetry affects stability as indicated in Fig. 9, where we have checked thoroughly the values of the function A for the equilibrium of Fig. 1. It turns out that at most of the upper parts of the equilibrium, where $y > 0$, A assumes small positive values, while for the lower part of the equilibrium ($y < 0$), it assumes small negative values. This slight A up-down asymmetry is connected to the respective slight asymmetry of the flux function u with respect to the vertical position y; the latter can be seen in Fig. 10, where the profile $u(x, y)$ is given at the point $x = 1 + x_s = 1.1$. Alhough $A < 0$, it does not necessarily imply an unstable equilibrium because the condition is sufficient, and the above result is consistent with the fact that up-down asymmetry may make the plasma unstable. For external modes this might relate to the vertical instability, e.g. Fitzpatrick (2011).

2. The nonlinearity favours the stability as shown in Fig. 11, where A is plotted as a function of x at the midplane $y = 0$ for the increasing values of the nonlinearity constant c_4.

https://doi.org/10.1017/S0022377813000883 Published online by Cambridge University Press

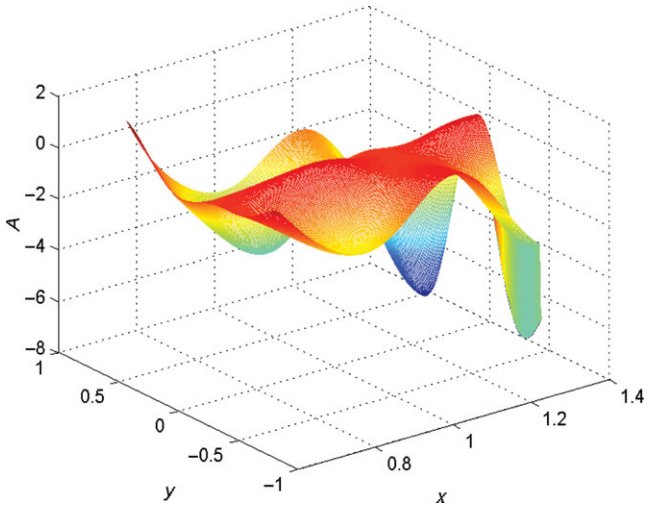


FIGURE 9. (Colour online) The stability function A for the equilibrium of Fig. 1. At the upper part ($y > 0$) of the equilibrium it mostly assumes positive values, while at the lower part ($y < 0$) it assumes negative values.

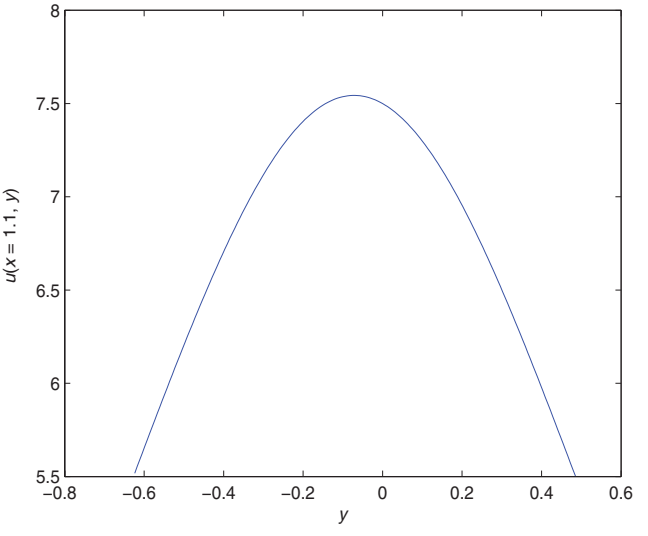


FIGURE 10. (Colour online) The poloidal magnetic flux function $u(x = 1.1, y)$ for the equilibrium of Fig. 1. It is slightly up-down asymmetric with respect to $y = 0$.

3. The flow has a slight stabilizing effect. An example is given in Fig. 12 in connection with the flow parameter M_{pa}.

6. Summary

We have constructed and studied nonlinear translational symmetric equilibria with strong reversed magnetic shear and sheared incompressible flow non-parallel to the magnetic field on the basis of the generalized Grad–Shafranov equation (1). This equation can be transformed to one identical in form with the static Grad–Shafranov equation, which we have solved in a couple of alternative ways (i) by using an ansatz for the unknown magnetic flux function (7) which reduces the original equation to a

https://doi.org/10.1017/S0022377813000883 Published online by Cambridge University Press

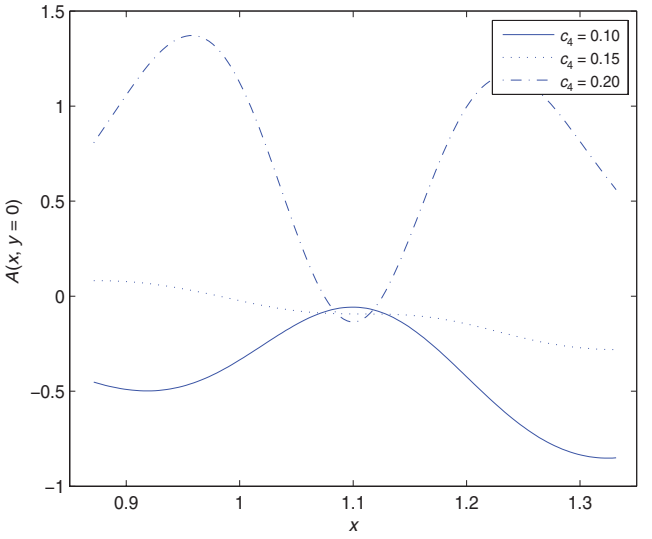


FIGURE 11. (Colour online) The stability function at the midplane $A(x, y = 0)$ for the equilibrium of Fig. 1 for various values of the nonlinear constant c_4. It appears that nonlinearity acts in favour of the stability.

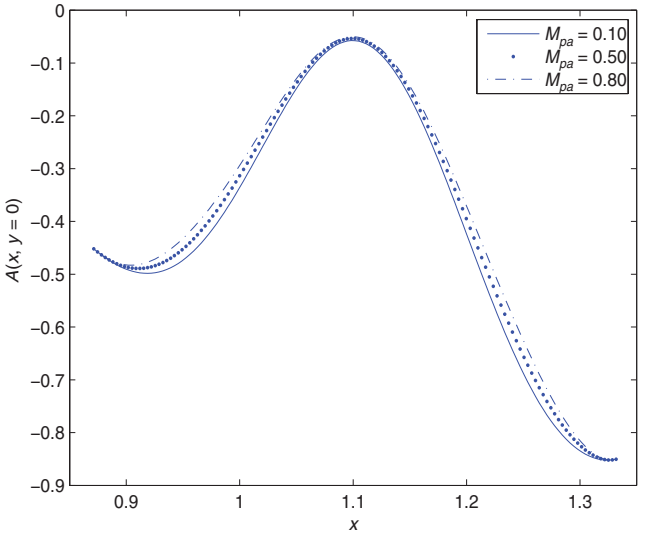


FIGURE 12. (Colour online) The stability function at the midplane $A(x, y = 0)$ for the equilibrium of Fig. 1 for various values of the flow parameter M_{pa}. It appears that flow acts in favour of the stability, although in a weak manner.

set of ODEs and algebraic constraints (9)–(14); then this set of equations is solved numerically, and (ii) full numerically by prescribing analytically a diverted boundary (17)–(20). The equilibria constructed are typically diamagnetic (Fig. 3), have peaked pressure profiles (Fig. 4), hollow toroidal current densities (Fig. 6), and electric fields possessing a maximum (Fig. 5). The maximum of **E** takes larger values as the flow amplitude increases but its position is insensitive to the flow.

For parallel flows application of a condition for linear stability implies that the equilibrium nonlinearity has a stabilizing effect together with a weaker stabilizing

https://doi.org/10.1017/S0022377813000883 Published online by Cambridge University Press

impact of the sheared flow in agreement with past nonlinear equilibrium studies (Throumoulopoulos et al. 2009; Throumoulopoulos and Tasso 2010; Kuiroukidis and Throumoulopoulos 2013). Also, even a small up-down asymmetry influences stability.

Finally, it would be interesting to try constructing equilibria with flow and reversed current density in connection with non-nested magnetic surfaces, thus generalizing the static ones of Martynov et al. (2003), Wang (2004) and Rodrigues and Bizzaro (2007) and extend the study to axially symmetric equilibria by possibly generalizing the ansatz (7) to examining the impact of toroidicity.

Aknowledgements

G. N. Throumoulopoulos would like to thank Henri Tasso and George Poulipoulis for useful discussions. The work leading to this paper was performed within the participation of the University of Ioannina in the Association Euratom-Hellenic Republic, which is supported in part by the European Union (Contract of Association No. ERB 5005 CT 99 0100) and by the General Secretariat of Research and Technology of Greece. The views and opinions expressed herein do not necessarily reflect those of the European Commission.

Appendix. Quantities appearing in the ODEs and algebraic constraints (10–14)

The functions $G_1,\ G_4,$ and G_5 appearing in (10)–(12) are given by

$$\begin{aligned} G_1 = & -4D_0D_1(N_2-f)+4D_1^2(N_1-fD_1) \\ & -6D_0(N_1-fD-1)-2D_0D_0^{'}(N_1^{'}-fD_1^{'}-f^{'}D_1) \\ & +2(D_0^{'})^2(N_1-fD_1)-2D_0^2D_1^{'}f^{'}+c_1D_0^2D_1+c_2D_0^2N_1 \\ & -c_3f^2D_0^2D_1+2c_3fD_0^2N1+3c_4f^2D_0^2N_1 \\ & -2c_4f^3D_0^2D_1, \end{aligned} \tag{A 1}$$

$$\begin{aligned} G_4 = & -2(N_2-f)+\frac{2D_1(N_1-fD_1)}{D_0}-2D_0^{'}(N_2^{'}-f^{'}) \\ & -2D_1^{'}(N_1^{'}+D_1N_2^{'}-N_2D_1^{'})+2c_1D_1^2+2c_2N_1D_1 \\ & +c_3N_1^2+2c_3fD_0N_2+2c_3N_1N_2D_1-c_3f^2D_0 \\ & -c_3N_2^2D_1^2-c_3D_0N_2^2-c_4f^3D_0-c_4N_2^3D_1^2 \\ & +3c_4fD_0N_2^2+3c_4N_2N_1^2-2c_4N_2^3D_0, \end{aligned} \tag{A 2}$$

$$\begin{aligned} G_5 = & -2D_1^{'}N_2^{'}+c_1D_1+c_2N_1+2c_3N_1N_2 \\ & -c_3N_2^2D_1-2c_4N_2^3D_1+3c_4N_1N_2^2. \end{aligned} \tag{A 3}$$

The functions $G_2,\ G_3$ appearing in (13)–(14) are given by

$$\begin{aligned} G_2 = & -2D_1^2(N_2-f)+\frac{2D_1^3(N_1-fD_1)}{D_0}+2c_1D_0D_1^2 \\ & -c_3f^2D_0D_1^2-c_4f^3D_0D_1^2-10D_0(N_2-f) \\ & +4D_1(N_1-fD_1)-c_3f^2D_0^2-2c_4f^3D_0^2 \\ & +2f^{'}D_0^{'}(D_1^2+2D_0)-2D_0^{'}(f^{'}D_0+fD_0^{'}) \\ & -2D_1D_1^{'}(f^{'}D_0+fD_0^{'})-c_3N_2^2D_0^2-c_4N_2^3D_0^2 \end{aligned}$$

https://doi.org/10.1017/S0022377813000883 Published online by Cambridge University Press

$$-2N_1^{'}D_0^{'}D_1 - 2N_1^{'}D_0D_1^{'} - 2N_2^{'}D_0D_0^{'} + 2fD_0(D_1^{'})^2$$
$$+2N_2(D_0^{'})^2 + 4N_1D_0^{'}D_1^{'} + 2c_2N_1D_0D_1$$
$$+2c_3fD_0D_1N_1 + c_3N_1^2D_0 + 2c_3fD_0^2N_2 + 3c_4fD_0N_1^2$$
$$+3c_4f^2D_0^2N_2 \tag{A 4}$$

and

$$G_3 = -4D_1(N_2 - f) + \frac{4D_1^2(N_1 - fD_1)}{D_0} - 2c_3f^2D_0D_1$$
$$-2c_4f^3D_0D_1 + 4D_1f^{'}D_0^{'} - 2c_3N_2^2D_0D_1 - 2c_4N_2^3D_0D_1$$
$$-2(f^{'}D_0 + fD_0^{'})D_1^{'} - 2N_1^{'}D_0^{'} - 2N_1^{'}D_1D_1^{'} - 2N_2^{'}D_0^{'}D_1$$
$$-2N_2^{'}D_0D_1^{'} + 2N_1(D_1^{'})^2 + 4N_2D_0^{'}D_1^{'} + 2N_1 - 2N_2D_1$$
$$+c_1D_1^3 + 2c_1D_0D_1 + c_2N_1D_1^2 + 2c_2N_1D_0 + 2c_3fD_0N_1$$
$$+c_3N_1^2D_1 + 2c_3fD_0D_1N_2 + +2c_3N_1N_2D_0$$
$$+c_4N_1^3 + 6c_4N_1N_2fD_{0.} \tag{A 5}$$

REFERENCES

Apostolaki, D., Throumoulopoulos, G. N. and Tasso, H. 2008 *35th EPS Conference on Plasma Physics*, Hersonissos, Crete, Greece, 9–13 June 2008, ECA Vol. 32 (ed. P. Lalousis and S. Moustaizis). European Physical Society, P-2.057.

Bellan, P. M. 2002 *Phys. Plasmas* **9**, 3050.

Clemente, R. A. and Farengo, R. 1984 *Phys. Fluids* **27**, 776.

de Vries, P. C., Joffrin, E., Brix, M., Challis, C. D., Crombé, K., Esposito, B., Hawkes, N. C., Giroud, C., Hobirk, J., Lönnroth, J., Mantica, P., Strintzi, D., Tala, T., Voitsekhovitch, I. and JET-EFDA Contributors to the Work Programme 2009 *Nucl. Fusion* **49**, 075007.

Fitzpatrick, R. 2011 *Nucl. Fusion* **51**, 053007.

Friedlander, S. and Vishik, M. M. 1995 *Chaos* **5**, 416.

Gerald, C. and Wheatley, P. 1989 *Applied Numerical Analysis*. Canada: Addison-Wesley.

Goedbloed, J. P. and Lifschitz, A. 1997 *Phys. Plasmas* **4**, 3544.

Gourdain, P.-A. and Leboeuf, J.-N. 2009 *Phys. Plasmas* **16**, 112506.

Greene, J. M. 1988 *Plasma Phys. Control. Fusion* **30**, 327.

Ilgisonis, V. I. and Pozdnyakov, Yu. I. 2002 *Plasma Phys. Reports* **28**, 83.

Khater, A. H. and Moawad, S. M. 2009 *Phys. Plasmas* **16**, 122506.

Kuiroukidis, A. 2010 *Plasma Phys. Control. Fusion* **52**, 015002.

Kuiroukidis, A. and Throumoulopoulos, G. N. 2012 *Phys. Plasmas* **19**, 022508.

Kuiroukidis, A. and Throumoulopoulos, G. N. 2013 *J. Plasma Phys.* **79**, 257.

Martins, C. G. L., Roberto, M., Caldas, I. L. and Braga, F. L. 2011 *Phys. Plasmas* **18**, 082508.

Martynov, A. A., Medvedev, S. Yu., Villard, L. 2003 *Phys. Rev. Lett.* **91**, 085004.

Mashke, E. K. and Perrin, H. 1984 *Phys. Lett.* A **102**, 106.

Rodrigues, P. and Bizzaro, J. P. S. 2007 *Phys. Rev. Lett.* **99**, 125001.

Shafer, M. W., McKee, G. R., Austin, M. E., Burrell, K. H., Fonck, R. J. and Schlossberg, D. J. 2009 *Phys. Rev. Lett.* **103**, 075004.

Shi, B. 2011 *Nucl. Fusion* **51**, 023004.

Simintzis, Ch., Throumoulopoulos, G. N., Pantis, G. and Tasso, H. 2001 *Phys. Plasmas* **8**, 2641.

Strumberger, E., Günter, S., Hobirk, J., Igochine, V., Merkl, D., Schwarz, E., Tichmann, C. and the ASDEX Upgrade Team 2004 *Nucl. Fusion* **44**, 464.

Tasso, H. and Throumoulopoulos, G. N. 1998 *Phys. Plasmas* **5**, 2378.

Throumoulopoulos, G. N. and Tasso, H. 1997 *Phys. Plasmas* **4**, 1492.

Throumoulopoulos, G. N. and Tasso, H. 2007 *Phys. Plasmas* **14**, 122104.

Throumoulopoulos, G. N. and Tasso, H. 2010 *Phys. Plasmas* **17**, 032508.

https://doi.org/10.1017/S0022377813000883 Published online by Cambridge University Press

Throumoulopoulos, G. N. and Tasso, H. 2012 *Phys. Plasmas* **19**, 014504.
Throumoulopoulos, G. N., Tasso, H. and Poulipoulis, G. 2009 *J. Phys. A: Math. Theor*. **42**, 335501.
Throumoulopoulos, G. N., Weitzner, H. and Tasso, H. 2006 *Phys. Plasmas* **13**, 122501.
Tsui, K. H., Navia, C. E., Serbeto, A. and Shigueoka, H. 2011 *Phys. Plasmas* **18**, 072502.
Vladimirov, V. A. and Ilin, K. I. 1998 *Phys. Plasmas* **5**, 4199.
Wang, S. 2004 *Phys. Rev. Lett*. **93**, 155007.
Wesson, J. 2011 *Tokamaks*, 4th edn., Oxford Engineering Science Series 149. Oxford, UK: Oxford University Press.

https://doi.org/10.1017/S0022377813000883 Published online by Cambridge University Press